Climate Dynamics (2021) 56:17–27
https://doi.org/10.1007/s00382-020-05325-z

Mechanisms of tropical precipitation biases in climate models

Hanjun Kim[1] · Sarah M. Kang[1] · Ken Takahashi[2] · Aaron Donohoe[3] · Angeline G. Pendergrass[4]

Received: 28 January 2020 / Accepted: 2 June 2020 / Published online: 27 October 2020

Abstract

We investigate the possible causes for inter-model spread in tropical zonal-mean precipitation pattern, which is divided into hemispherically symmetric and anti-symmetric modes via empirical orthogonal function analysis. The symmetric pattern characterizes the leading mode and is tightly related to the seasonal amplitude of maximum precipitation position. The energetic constraints link the symmetric pattern to the seasonal amplitude in cross-equatorial atmospheric energy transport AET_0 and the annual-mean equatorial net energy input NEI_0. Decomposition of AET_0 into the energetics variables indicates that the inter-model spread in symmetric precipitation pattern is correlated with the inter-model spread in clear-sky atmospheric shortwave absorption, which most likely arises due to differences in radiative transfer parameterizations rather than water vapor patterns. Among the components that consist NEI_0, the inter-model spread in symmetric precipitation pattern is mostly associated with the inter-model spread in net surface energy flux in the equatorial region, which is modulated by the strength of cooling by equatorial upwelling. Our results provide clues to understand the mechanism of tropical precipitation bias, thereby providing guidance for model improvements.

Keywords Tropical precipitation · Model uncertainty · Double ITCZ problem · Energetic constraints · Cold tongue bias · Atmospheric shortwave absorption

1 Introduction

Most of the state-of-the-art coupled general circulation models (CGCM) overestimate precipitation south of the equator and underestimate it near the equator: this bias is termed as the double intertropical convergence zone (ITCZ) problem (Mechoso et al. 1995; Lin 2007). Despite steady improvements in resolution and model parameterizations, the double ITCZ problem has been persistent in CGCMs across generations of climate models (Zhang et al. 2015). This model bias in tropical precipitation has various climatic consequences. For example, Ham and Kug (2014) showed that the climate models with excessive precipitation over the central/eastern Pacific ITCZ tend to simulate a slower phase transition of the El Niño-Southern Oscillation; Tian (2015) found that the double ITCZ bias is negatively correlated with the degree of global surface warming following a doubling of CO_2, namely equilibrium climate sensitivity; Zhou and Xie (2015) demonstrated that the projected tropical climate change is sensitive to the double ITCZ bias in the mean state. Thus, identifying the possible causes of the double ITCZ bias is of critical importance not only to correctly simulate the current climate state but also for a more reliable future climate projection.

Previous studies attribute the double ITCZ bias to local processes such as poor representation of tropical ocean–atmosphere feedback (Lin 2007; Li and Xie 2014), improper entrainment rate (Hirota et al. 2011), biased sea surface temperature (SST) threshold for onset of convection (Bellucci et al. 2010; Oueslati and Bellon 2015), inappropriate wind strength in the eastern Pacific and coastal

Electronic supplementary material The online version of this article (https://doi.org/10.1007/s00382-020-05325-z) contains supplementary material, which is available to authorized users.

✉ Sarah M. Kang
skang@unist.ac.kr

[1] School of Urban and Environmental Engineering, Ulsan National Institute of Science and Technology, UNIST-gil 50, Ulsan 689-798, Republic of Korea

[2] Servicio Nacional de Meteorología e Hidrología del Perú (SENAMHI), Lima, Peru

[3] Applied Physics Laboratory, University of Washington, Seattle, WA, USA

[4] National Center for Atmospheric Research, Boulder, CO, USA

regions (de Szoeke and Xie 2008; Zheng et al. 2011), and convection scheme (Song and Zhang 2018). The recently developed framework that links the ITCZ position to the inter-hemispheric atmospheric energy contrast (Broccoli et al. 2006; Kang et al. 2008; Schneider et al. 2014; Kang 2020) has led a line of research to look for possible causes of the double ITCZ problem from biases in the atmospheric energy budget. The energetic framework provides different mechanisms for hemispherically anti-symmetric tropical precipitation biases—characterized by the precipitation difference between the tropics in the Northern Hemisphere (NH) and Southern Hemisphere (SH)—and hemispherically symmetric tropical precipitation biases—characterized by the meridional width of the intense equatorial precipitation.

In particular, hemispherically symmetric biases in tropical precipitation have been linked to the biases in the equatorial net energy input (NEI_0) into the atmospheric column: a larger NEI_0 is associated with more equatorial precipitation and vice versa (Adam et al. 2017). The NEI_0 biases in turn have been related to the cold tongue biases over the eastern equatorial Pacific. In contrast, hemispherically anti-symmetric biases in tropical precipitation have been linked to biases in the cross-equatorial atmospheric energy transport (Adam et al. 2016b). For example, the lack of clouds over the Southern Ocean can result in anomalously northward atmospheric energy transport across the equator that is accompanied by excessive precipitation south of the equator, and hence the Southern Ocean cloud bias has been suggested to contribute to hemispherically anti-symmetric biases in tropical precipitation (Hwang and Frierson 2013). However, the degree to which a Southern Ocean cloud bias correction in CGCMs improves the tropical precipitation bias turns out to be highly model dependent (Kay et al. 2016; Mechoso et al. 1995; Hawcroft et al. 2017). Causes for the inter-model diversity will be investigated within the recently initiated Extratropical-Tropical Interaction Model Intercomparison Project, namely ETIN-MIP (Kang et al. 2019). In fact, more recent studies have found that hemispherically anti-symmetric biases in tropical precipitation are not significantly correlated with extratropical energetic biases but tightly linked to the tropical net surface energy biases (Xiang et al. 2017), which can be traced to land surface temperature biases (Zhou and Xie 2017).

The tropical precipitation biases can be characterized in a number of different ways. The most common measure is the southern ITCZ index, which is the climatological mean precipitation bias over the southeastern Pacific (Bellucci et al. 2010). Another frequently used measure for quantifying the hemispherically anti-symmetric component of the zonal-mean tropical precipitation is the precipitation asymmetry index (PAI), which is the precipitation difference between northern (0°–20° N) and southern tropics (20° S–0°) normalized by the tropical-mean (20° S–20° N) (Hwang and Frierson 2013). The hemispherically symmetric component is quantified by the equatorial precipitation index (E_p), which is the equatorial (2° S–2° N) precipitation divided by the tropical-mean (20° S–20° N) subtracted from unity (Adam et al. 2016b). Because each index characterizes distinct aspects of the tropical precipitation pattern, it is difficult to reconcile how they each contribute to the behavior of the overall tropical precipitation pattern.

In this study, we characterize the tropical precipitation distribution in a more objective manner based on an inter-model Empirical Orthogonal Function (EOF) analysis of zonal-mean tropical precipitation. The inter-model spread of zonal-mean tropical precipitation is largely divided into the two components, which respectively characterize the meridional width and hemispheric contrast of tropical precipitation. Independence of the two components indicates they may be governed by distinct mechanisms. We proceed to identify the leading pattern of inter-model spread and investigate its source based on the energetic constraints.

2 Methodology and data

2.1 Energetic constraints on the ITCZ position

The ITCZ is associated with a low-level wind convergence and an upper-level wind divergence, coinciding with the ascending branch of the Hadley Circulation (HC). Provided that the HC ascending branch is vertically straight and that eddy fluxes contribute little to energy transport, the zonal-mean ITCZ location is associated with the so-called "energy flux equator" (EFE) where the atmospheric energy transport vanishes (Kang et al. 2008, 2009; Donohoe et al. 2013; Adam et al. 2016a).

The vertically integrated moist static energy transport in the atmosphere (AET) can be linked to net energy input (NEI) into the atmospheric column (Neelin and Held 1987) via the atmospheric energy budget:

$$\nabla \cdot \mathrm{AET} = \mathrm{NEI} - \frac{d}{dt}\int_0^{P_s} \left(C_p T + L_v q\right)\frac{dP}{g} \tag{1}$$

where $\mathrm{NEI} = \mathrm{SW}^{\downarrow}_{\mathrm{NET,TOA}} - \mathrm{LW}^{\uparrow}_{\mathrm{NET,TOA}} + \mathrm{SH}^{\uparrow}_{\mathrm{SFC}} + \mathrm{LH}^{\uparrow}_{\mathrm{SFC}} - \mathrm{SW}^{\downarrow}_{\mathrm{NET,SFC}} + \mathrm{LW}^{\uparrow}_{\mathrm{NET,SFC}}$ is the sum of vertical energy fluxes from the top-of-atmosphere (TOA) and the surface. The TOA energy fluxes consist of net downward shortwave flux ($\mathrm{SW}^{\downarrow}_{\mathrm{NET,TOA}}$) minus net upward longwave flux ($\mathrm{LW}^{\uparrow}_{\mathrm{NET,TOA}}$); the surface energy fluxes consist of upward sensible heat flux ($\mathrm{SH}^{\uparrow}_{\mathrm{SFC}}$), upward latent heat flux ($\mathrm{LH}^{\uparrow}_{\mathrm{SFC}}$), and net upward longwave flux ($\mathrm{LW}^{\uparrow}_{\mathrm{NET,SFC}}$) minus net downward shortwave flux ($\mathrm{SW}^{\downarrow}_{\mathrm{NET,SFC}}$). P_s is the surface pressure, T is the atmospheric temperature, and q is the specific humidity, with the constants C_p, the heat capacity at constant pressure, and L_v, the latent heat of vaporization for water. The second term on the right-hand side is the time tendency in vertical integral

of atmospheric moist enthalpy, which represents energy storage in the atmosphere. Note that all quantities are zonally averaged.

By applying the first-order Taylor expansion of AET at the equator and substituting Eq. (1) for the divergence of AET, we obtain an expression for the energy flux equator and thus the ITCZ position (Schneider et al. 2014; Adam et al. 2016a):

$$\begin{aligned} \mathrm{EFE} \cong \tilde{\phi}_{\mathrm{ITCZ}} &= -\frac{\mathrm{AET}_0}{\partial_\phi(\mathrm{AET})_0} \\ &= -\frac{\mathrm{AET}_0}{\mathrm{NEI}_0 - \left(\frac{d}{dt}\int_0^{P_s}\left(C_pT + L_vq\right)\frac{dP}{g}\right)_0} \\ &\cong -\frac{\mathrm{AET}_0}{\mathrm{NEI}_0} \end{aligned} \tag{2}$$

where the subscript 0 denotes the equatorial values. Following Adam et al. (2016a), the time tendency of atmospheric energy storage term near the equator is neglected since it is small relative to NEI_0.

2.2 Data and analysis method

We examine the monthly data of historical simulations from 13 CMIP3, 35 CMIP5, and 25 CMIP6 models (Table S1) (Meehl et al. 2007; Taylor et al. 2012; Eyring et al. 2016). We only use the first ensemble member for each model. NEI is calculated as the sum of downward net TOA radiation and upward net surface energy flux. AET is calculated by taking the spatial integral of the right-hand side of Eq. (1) over the Southern Hemisphere, after subtracting the global-mean. We adopt this indirect method for estimating AET_0 because the temporal resolution is too coarse to resolve transient eddies.

The observed climate features are characterized by two datasets for precipitation: Global Precipitation Climatology Project (GPCP) (Adler et al. 2003) and Climate Prediction Center (CPC) merged analysis precipitation (CMAP) product (Xie and Arkin 1997). Although CMAP is partially obtained from the NCEP/NCAR reanalysis data, we use both GPCP and CMAP in an effort to represent uncertainty in observations. In contrast to the models, we use a direct method for calculating the observed estimate of AET using four-times daily European Center for Medium-Range Weather Forecasts (ECMWF) Interim Reanalysis (ERA-Interim) product (Dee et al. 2011). When calculating AET, winds are first forced to balance the atmospheric mass budget with a barotropic wind correction as in Trenberth (1997). The corrected winds are used to calculate the meridional flux of moist static energy, which is then vertically integrated to derive AET. The observed estimate of NEI is obtained as the sum of atmospheric heat storage and AET divergence, following Eq. (1).

Both CMIP and observations are analyzed for the 20-year period from 1980 to 1999 and interpolated to a common $1^\circ \times 1^\circ$ grid. In both cases, the NEI_0 is calculated as the area-average over 6° S–6° N. While the exact value of NEI_0 is sensitive to the meridional boundary of integration, it does not affect the qualitative features of our results.

3 Results

3.1 Characterizing inter-model spread in zonal- and annual- mean tropical precipitation

We first normalize each model's precipitation by its tropical-mean value (20° S–20° N) to highlight the difference in spatial pattern across models (Fig. 1a). The multi-model-mean (black) is biased compared to observations (colors): models produce relatively less precipitation near and north of the equator and relatively more precipitation in the southern tropics, which is the well-known double-ITCZ bias. Notably, the inter-model spread of normalized tropical precipitation is so large that it is substantially larger than the bias of multi-model-mean from observations.

To objectively characterize the inter-model spread, we apply an inter-model EOF analysis to the normalized zonal-mean tropical precipitation. The two observations are included when performing the EOF analysis in order to elucidate how each model is biased relative to the observational estimates. The EOF analysis results with and without the observations are essentially indistinguishable. The first two modes explain 77% of the spread (Fig. 1b). The first mode (denoted TOT1, red dashed) is nearly symmetric about the equator, whereas the second mode (denoted TOT2, blue dashed) is anti-symmetric about the equator. To more cleanly separate the symmetric and anti-symmetric components of spread, we separately apply an inter-model EOF analysis to the hemispherically symmetric and anti-symmetric components of normalized tropical precipitation. The first mode of symmetric component is denoted as SYM1 and the corresponding principal component as SYM1 -PC. Conversely, the first mode of anti-symmetric component is denoted as ASY1 and the corresponding principal component as ASY1-PC. As expected, SYM1-PC exhibits a high correlation of 0.91 with the equatorial precipitation index (E_p), which quantifies the hemispherically symmetric component in Adam et al. (2016b) (Fig. S1a); meanwhile, ASY1-PC exhibits a high correlation of 0.98 with the tropical precipitation asymmetry index (*PAI*), which quantifies the hemispherically anti-symmetric component in Hwang and Frierson (2013) (Fig. S1b). The meridional profile of SYM1 is close to that of TOT1 while the meridional pattern of ASY1 is close to that of TOT2 (Fig. 1b). High correlation between the corresponding PCs (Fig. S1c-d) indicates that

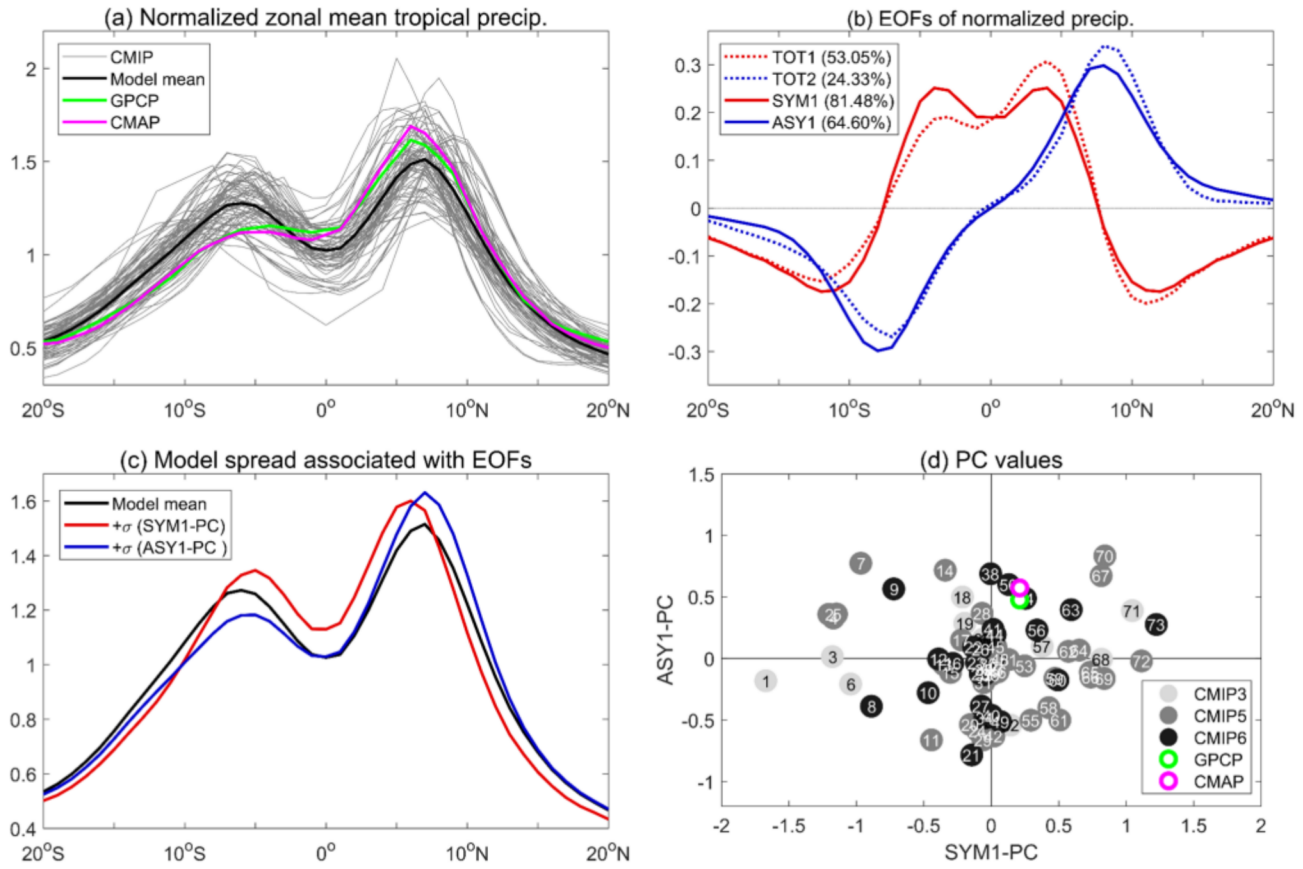

Fig. 1 **a** Annual- and zonal- mean tropical precipitation normalized by tropical-mean (20° S–20° N) in observations (colors), CMIP models (gray), and multi-model-mean (black) (unitless). **b** The first (TOT1; red dashed) and second (TOT2; blue dashed) mode of inter-model variability from the EOF analysis of both modeled and observed precipitation in **a**, and the first mode of the hemispherically symmetric (SYM1; red solid) and anti-symmetric (ASY1; blue solid) components of **a**. The fraction of explained variance of each mode is shown in the legend. **c** Multi-model-mean of normalized tropical precipitation (black) and that added to one positive standard deviation of SYM1-PC (red) and ASY1-PC (blue). **d** The SYM1-PC (x-axis) versus ASY1-PC (y-axis) for CMIP3 (light gray), CMIP5 (dark gray), and CMIP6 (black) models. Model numbers increase in the order of SYM1-PC and the model name corresponding to each number is offered in Table S1. Colored circles represent observational estimations from GPCP (green) and CMAP (magenta)

TOT1 and TOT2 correspond to SYM1 and ASY1, respectively. That is, the first two EOFs of normalized tropical precipitation across models and observations are nearly identical to the hemispherically symmetric and anti-symmetric components. By construction, the EOFs TOT1 and TOT2 are orthogonal just as, by geometric arguments, ASY1 and SYM1 are orthogonal. In this sense, SYM1 and ASY1 can be thought of as an alternative basis for describing tropical precipitation biases with only a slight loss of optimization for variance explained in the EOF basis. Hereafter, we examine SYM1 and ASY1..

SYM1, which explains about 53% of the total inter-model variability of normalized tropical precipitation, is characterized by an equatorward squeeze of tropical precipitation (red in Fig. 1c). SYM1 PC is more negative in most models compared to observations (Fig. 1d), indicative of deficient precipitation near the equator and excessive precipitation off the equator, consistent with the bias of normalized tropical precipitation in Fig. 1a. ASY1, which explains about 24% of the total inter-model variability, is characterized by a northward shift of tropical precipitation (blue in Fig. 1c). Most models have smaller ASY1-PC values than observations (Fig. 1d), indicative of more precipitation in the southern tropics than in the northern tropics relative to observations, consistent with Fig. 1a.

In the following analysis, we focus on the examination of SYM1, which is the leading mode of inter-model variability of normalized tropical precipitation. We compare the monthly precipitation climatology of ten models of the lowest SYM1-PC values (Fig. 2a) and ten models of the highest SYM1-PC values (Fig. 2b). The latitude of maximum precipitation extends farther poleward throughout the year for ten models of the lowest SYM1-PC values than those of the highest. Hence, the pattern of monthly normalized zonal mean tropical precipitation regressed onto SYM1-PC exhibits an equatorial squeeze of tropical

precipitation throughout the year (Fig. 2c). That is, models with larger relative annual-mean precipitation in the equatorial band would exhibit a smaller amplitude of the seasonal cycle of the ITCZ position. To quantify this relationship, we measure the seasonal amplitude of the ITCZ position as $Amp(\emptyset_{ITCZ}) \equiv \sqrt{\sum_{i=1}^{i=12} \left(\emptyset_{ITCZ}^{i} - \bar{\emptyset}_{ITCZ}\right)^2}$ where $\emptyset_{ITCZ}^{i}$ is the latitude of maximum zonal-mean precipitation at the ith month and $\bar{\emptyset}_{ITCZ}$ is annual-mean value. Figure 2d shows that $Amp(\emptyset_{ITCZ})$ is strongly correlated with SYM1-PC ($r = -0.89$), which implies that the inter-model spread in the hemispherically symmetric component of annual- and zonal-mean tropical precipitation is associated with the seasonal amplitude of the ITCZ position. Thus, in the next section, we examine the factors contributing to the inter-model spread in the seasonal amplitude of the ITCZ position.

3.2 Application of the energetic constraints

The atmospheric energy budget in Eq. (2) allows us to attribute the monthly variation in the ITCZ position to the monthly variation of AET_0 and/or NEI_0: a more equatorward ITCZ is associated with a smaller AET_0 and/or a larger NEI_0 and vice versa for a more poleward ITCZ. Hence, the models with a smaller seasonal cycle of the ITCZ (i.e., larger SYM1 -PC values) exhibit a smaller seasonal amplitude of AET_0 and a larger NEI_0 for all months compared to the models with a larger seasonal cycle of the ITCZ (i.e., smaller SYM1 -PC values) (Fig. S2).

The seasonal amplitude of AET_0 is calculated as $Amp(AET_0) \equiv \sqrt{\sum_{i=1}^{i=12} \left(AET_0^{i} - \overline{AET_0}\right)^2}$ where AET_0^{i} is the cross-equatorial AET at the ith month and $\overline{AET_0}$ is annual-mean value. A smaller $Amp(AET_0)$ is associated

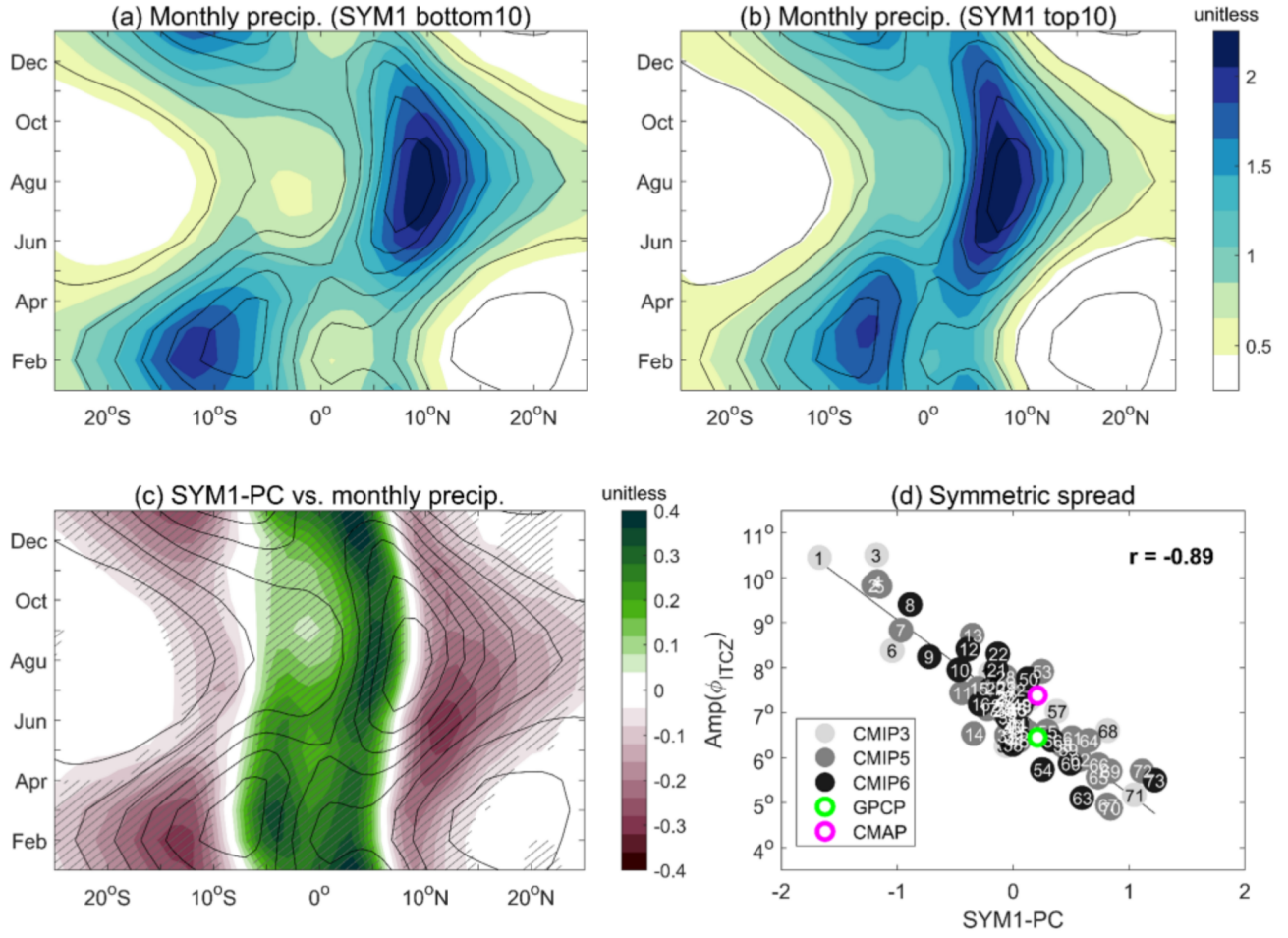

Fig. 2 Hovmöller diagram of monthly normalized precipitation composites (shading) of **a** 10 models with the lowest SYM1-PC and **b** 10 models with the highest SYM1-PC, with the multi-model-mean of all available 73 models (contour; interval = 0.25 mm day^{-1}). **c** The inter-model linear regression map of monthly precipitation onto SYM1-PC (shading). Black contour is the same as in **a**, **b**. Hatching indicates where the regression coefficient is significantly different from zero at the 95% confidence level using a two-sided Student's t test. **d** Scatter plot between SYM1-PC and the seasonal amplitude of monthly ITCZ, $Amp(\emptyset_{ITCZ})$, with the correlation coefficient indicated in the upper right corner

with a smaller seasonal amplitude of the ITCZ position (Fig. S2a), leading to an equatorward squeeze of the annual-mean normalized tropical precipitation, reflected as a larger SYM1-PC. Indeed, $Amp(\mathrm{AET}_0)$ is negatively correlated to SYM1-PC, with $r=-0.48$ (Fig. 3a). A larger NEI_0 is associated with the ITCZ closer to the equator for all months (Fig. S2b), hence, the annual-mean NEI_0 is positively correlated with SYM1-PC with $r=0.48$ (Fig. 3b). Note that the annual-mean NEI_0 is used here because the inter-model spread in NEI_0 exhibits little seasonality (Fig. S2b). Guided by the approximation in Eq. (2), we measure the correlation between SYM1-PC and $\frac{Amp(\mathrm{AET}_0)}{\text{annual-mean}(\mathrm{NEI}_0)}$ (Fig. 3c). When both $Amp(\mathrm{AET}_0)$ and the annual-mean NEI_0 are considered, the correlation coefficient is higher ($r=-0.78$) than when either factor is individually considered, implying that both factors contribute to the spread in SYM1-PC. We now investigate possible controlling factors of $Amp(\mathrm{AET}_0)$ and the annual-mean NEI_0, respectively.

3.2.1 Effect of spread of monthly variations in AET_0 on tropical precipitation

Equation (1) indicates that the seasonal variations in AET_0 are determined by the hemispheric asymmetry in NEI and atmospheric energy storage (STOR_{atm}). Following Donohoe et al. (2013), we rearrange NEI as the sum of the shortwave radiation absorbed in the atmosphere ($\mathrm{SWABS}=\mathrm{SW}^{\downarrow}_{\mathrm{NET,TOA}}-\mathrm{SW}^{\downarrow}_{\mathrm{NET,SFC}}$), energy fluxed from the surface to the atmosphere ($\mathrm{SE}=\mathrm{SH}^{\uparrow}_{\mathrm{SFC}}+\mathrm{LH}^{\uparrow}_{\mathrm{SFC}}+\mathrm{LW}^{\uparrow}_{\mathrm{NET,SFC}}$), and outgoing longwave radiation (OLR). Such rearrangement is motivated by the fact that the atmosphere is heated by the direct solar absorption within the atmosphere SWABS and the non-solar energy exchange between the surface and the atmosphere SE (Donohoe and Battisti 2013).

The monthly variation of the hemispheric contrast in each term (Fig. S3a) is regressed onto SYM1-PC (Fig. S3b). Among the four terms, the seasonal amplitude of hemispheric asymmetry in atmospheric shortwave absorption, denoted as $Amp\langle\mathrm{SWABS}\rangle$ where $\langle\rangle$ indicates the hemispheric contrast, is most strongly correlated to SYM1-PC with $r=-0.50$ (Fig. 4a). Furthermore, most spread in SWABS congruent with SYM1-PC originates from the clear-sky component $\mathrm{SWABS}_{\mathrm{clr}}$ rather than the cloud radiative effect $\mathrm{SWABS}_{\mathrm{cre}}$ (Fig. S3b).

The regression map of $\mathrm{SWABS}_{\mathrm{clr}}$ onto SYM1-PC for boreal summer (May–June–July) and austral summer (November–December–January) is shown as shading in Fig. 4b, c, respectively. The models with larger SYM1-PC values tend to have less clear-sky shortwave absorption over the entire globe, with the most pronounced effect in the summer hemisphere. Less $\mathrm{SWABS}_{\mathrm{clr}}$ in the summer hemisphere than the winter hemisphere would act to reduce the hemispheric contrast in NEI, requiring less atmospheric energy transport toward the winter hemisphere, thereby placing the ITCZ more toward the equator. The inter-model spread of $\mathrm{SWABS}_{\mathrm{clr}}$ is especially pronounced in the subtropics of the summer hemisphere where the climatological $\mathrm{SWABS}_{\mathrm{clr}}$ is maximized (colored contours in Fig. 4b, c). Hence, the hemispheric asymmetry of $\mathrm{SWABS}_{\mathrm{clr}}$ is proportional to the global- and annual-mean $\mathrm{SWABS}_{\mathrm{clr}}$ (Fig. S4a). The inter-model spread of $\mathrm{SWABS}_{\mathrm{clr}}$ presumably originates from model differences in water vapor distribution and/or

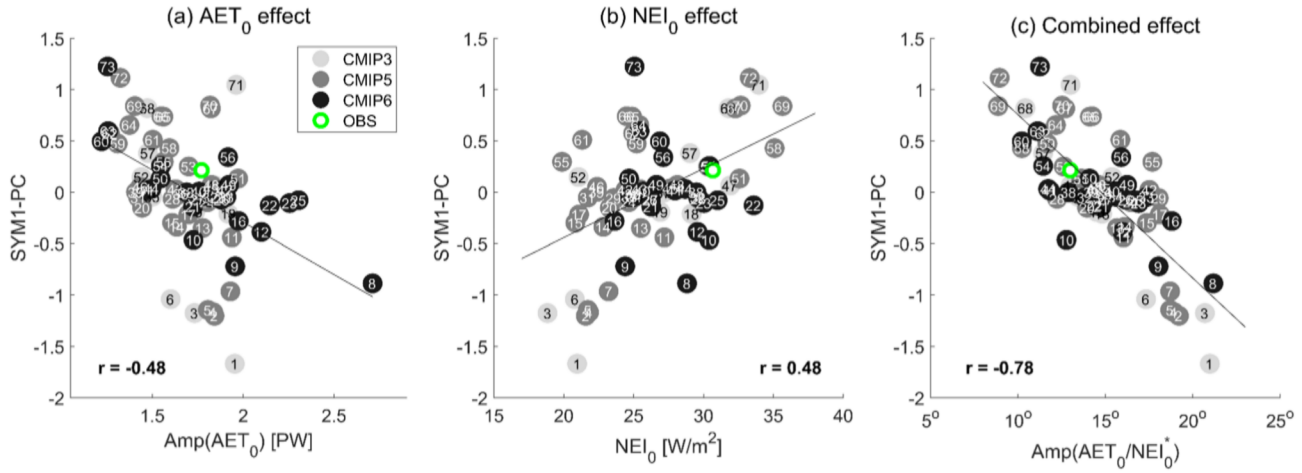

Fig. 3 Scatter plot between SYM1-PC and **a** the seasonal amplitude of cross-equatorial atmospheric energy transport $Amp(\mathrm{AET}_0)$, **b** the annual-mean NEI_0, and **c** the estimate of seasonal amplitude of ITCZ position from the energetic constraints, i.e., $Amp(\mathrm{AET}_0)/\mathrm{NEI}_0^*$ where NEI_0^* is the annual-mean NEI_0 whose unit is converted from W/m^2 to PW/1°. The green circle denotes the observed values: SYM1-PC on the ordinate from GPCP and the energetic variables on the abscissa from ERA-interim. The correlation coefficients are shown as bold text in each panel. All correlation coefficients are significantly different from zero according to a t-test at 95% confidence level

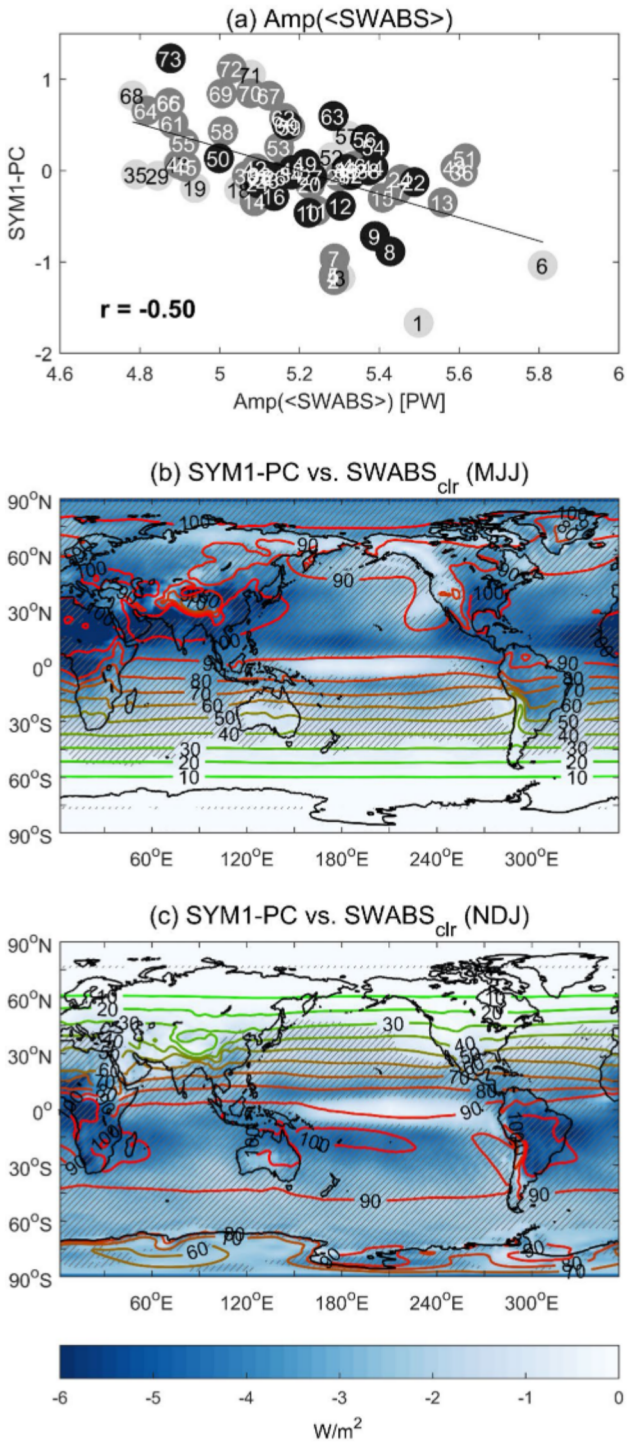

Fig. 4 **a** Scatter plot between the seasonal amplitude of SWABS and SYM1-PC. Inter-model regression map of $SWABS_{clr}$ onto SYM1-PC (shading) and the multi-model-mean climatology of $SWABS_{clr}$ with a contour interval of 10 W/m^2 (colored contour) for **b** May–June–July and **c** November–December–January. In **b**, **c**, the values that are significantly different from zero according to a t-test at 95% confidence level are hatched and 66 subsets of CMIP models in which $SWABS_{clr}$ are made available are used for the analysis (Table S1)

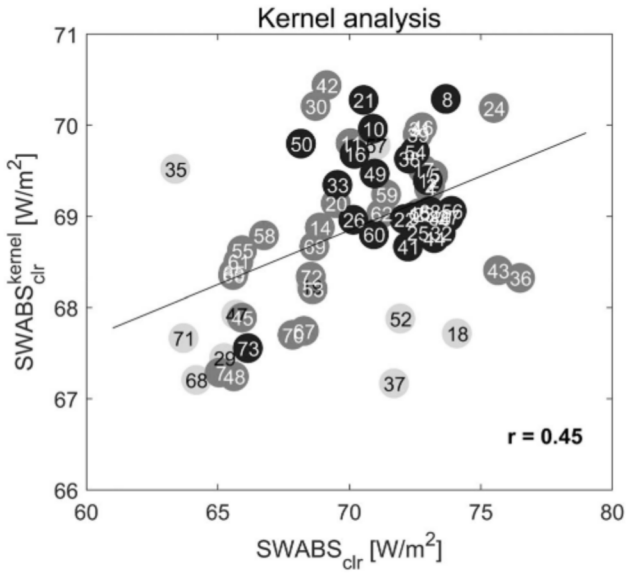

Fig. 5 Scatter plot between the annual- and global-mean $SWABS_{clr}$ and its estimation using the moisture and albedo kernels, i.e., $SWABS_{clr}^{kernel}$

shortwave parameterizations (Takahashi 2009; Pendergrass and Hartmann 2014) since 72% of atmospheric shortwave is absorbed by water vapor under cloud-free conditions (Collins et al. 2006).

To differentiate the effect of water vapor distribution from parameterization, we employ radiative kernels from the Community Earth System Model 1.1.2 (Pendergrass et al. 2018). The clear-sky shortwave moisture kernel for TOA and surface is applied for each spatial grid and each month, which is then multiplied by the corresponding inter-model spread of logarithm of specific humidity. The effect of albedo spread is also calculated and included in the estimation of $SWABS_{clr}$ but has an almost negligible effect (not shown). The vertically integrated and globally averaged values of the actual $SWABS_{clr}$ and the estimation from the kernel (denoted as $SWABS_{clr}^{kernel}$) are compared in Fig. 5. The radiative kernel analysis indicates that the inter-model spread in neither water vapor distribution nor albedo explains the inter-model spread in $SWABS_{clr}$, as can be seen from a much smaller range of $SWABS_{clr}^{kernel}$ than $SWABS_{clr}$ (Fig. 5). Note that the scale of ordinate is 5 times smaller than the scale of abscissa. Ruling out the effect of model differences in water vapor distribution, a plausible alternative cause for the inter-model spread in $SWABS_{clr}$ is differences in radiative transfer parameterizations, such as spectral resolution or extinction coefficient for water vapor. This speculation is supported by Pincus et al. (2015) that shows model differences in radiation parameterization produce large errors in shortwave absorption that outweigh the impact of model differences in atmospheric states, by performing

calculations with radiative transfer codes extracted from host CMIP models.

3.2.2 Effect of spread of annual-mean NEI_0 on tropical precipitation

Among the components of NEI_0, the equatorial annual-mean net surface heat flux ($SFC_0 = SH_0^{\uparrow} + LH_0^{\uparrow} - SW_{NET,0}^{\downarrow} + LW_{NET,0}^{\uparrow}$) is most strongly correlated with SYM1-PC at 0.57 (Fig. 6a). The regression map of the annual-mean SFC onto SYM1-PC (shading in Fig. 6b) reveals a large inter-model diversity of SFC congruent with SYM1-PC on the equatorial Pacific and Atlantic. Less downward surface energy flux near the equator is straddled by less upward surface energy flux in the subtropics, indicative of weaker oceanic heat transport (Boccaletti et al. 2004). This suggests that SYM1-PC is associated with the strength of the cold tongue, which is supported by the regression map of normalized SSTs (i.e., SSTs of each model normalized by the average SST between 20° S and 20° N) onto SYM1-PC (contour in Fig. 6b). That is, the models with more equatorially focused precipitation show a relatively warmer equatorial upwelling region thus weaker cold tongue strength, which is associated with the ineffective oceanic heat transport from the tropics to the subtropics.

To examine whether oceanic processes play an essential role in determining the inter-model spread of SFC congruent with SYM1-PC, we additionally analyze 48 AMIP experiments for the same period. In AMIP with prescribed SSTs and sea ice, the SFC regression map no longer shows a significant upward net surface flux in the equatorial Pacific (contrast Fig. 6b, c). This implies that model differences in atmospheric components may not be the cause of inter-model diversity of SFC_0 in the Pacific. Thus, the inter-model spread of the Pacific cold tongue strength associated with SYM1-PC could be attributed to model differences in the ocean dynamics or atmosphere–ocean coupling effect, consistent with Li et al. (2015) who suggest that the excessive cold tongue bias could be traced back to a strong oceanic dynamic cooling linked to shallow thermocline along the equatorial Pacific.

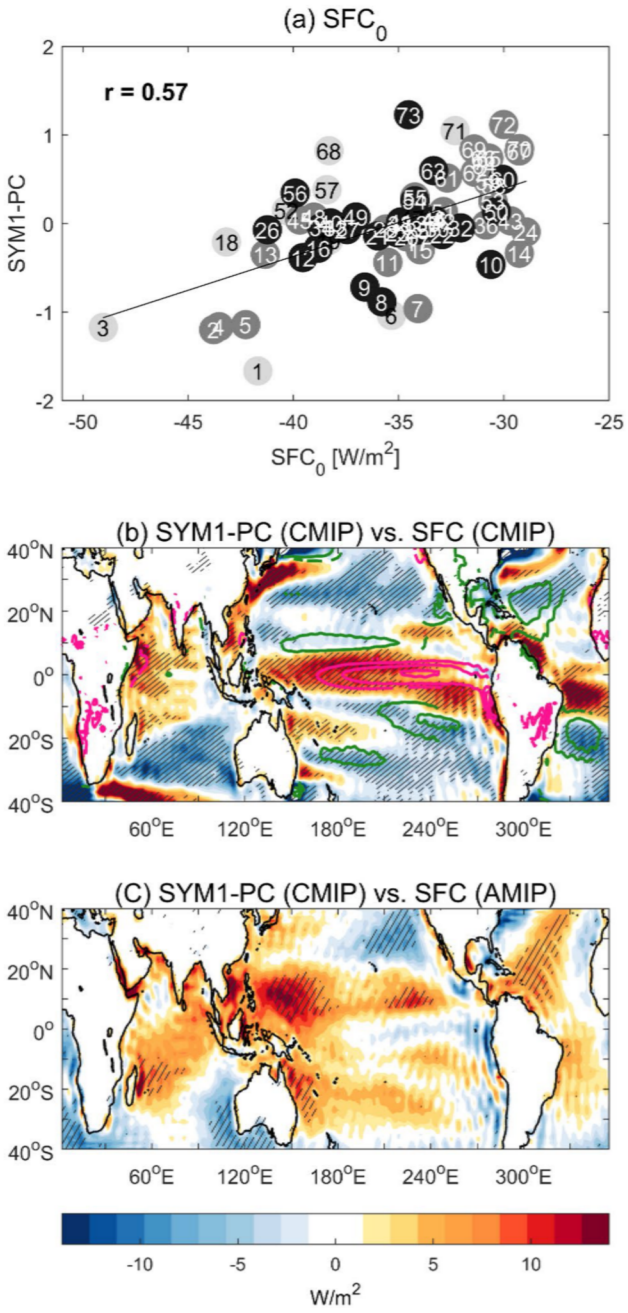

Fig. 6 **a** Scatter plot between the annual-mean upward positive net surface energy flux averaged between 6° S and 6° N (SFC_0) and SYM1-PC. **b** Inter-model regression map of annual-mean net surface energy flux onto SYM1-PC (shading) and inter-model regression map of normalized tropical SST onto SYM1-PC (colored contour) from CMIP models. Only statistically significant values are shown as contour, with positive values in pink and negative values in green. The contour interval is 3×10^{-4} (unitless). **c** Inter-model regression map of net surface energy flux from AMIP onto SYM1-PC from CMIP. In **b**, **c**, the statistically significant values are hatched as in Fig. 4

4 Summary and discussions

In this study, we investigate the possible causes for the inter-model spread and bias in the present-day zonal-mean tropical precipitation pattern. The inter-model EOF analysis is applied to the zonal-mean tropical precipitation patterns of models and observations. The first two modes closely resemble the hemispherically symmetric (SYM1) and anti-symmetric (ASY1) components, which respectively explain 53.0% and 24.3% of the total variance of precipitation spread. The orthogonality of EOFs implies that SYM1 and ASY1 originate from independent mechanisms. The leading mode (SYM1) is associated with the amplitude of monthly

variations in maximum precipitation position (i.e., ITCZ location). Based on the energetic framework linking the ITCZ position to the atmospheric energy budget, SYM1 is related to both the seasonal amplitude of cross-equatorial atmospheric energy transport $Amp(\mathrm{AET}_0)$ and the annual-mean net energy input into the equatorial atmosphere column NEI_0. Accurately speaking, the atmospheric energetic budget offers a proxy for the energy flux equator, not the ITCZ position itself; however, the energetic proxy value $\frac{Amp(\mathrm{AET}_0)}{\mathrm{annual-mean}(\mathrm{NEI}_0)}$ and actual ITCZ position $Amp(\emptyset_{\mathrm{ITCZ}})$ are highly correlated with the coefficient of 0.73 and the regression slope of 0.32 (Fig. S5).

Among the components of AET_0, the seasonal amplitude in the clear-sky SW atmospheric absorption $(\mathrm{SWABS}_{\mathrm{clr}})$ is most strongly correlated with SYM1-PC. The pattern of $\mathrm{SWABS}_{\mathrm{clr}}$ regressed onto SYM1-PC reveals that the models with a smaller annual- and global-mean $\mathrm{SWABS}_{\mathrm{clr}}$ are associated with a weaker amplitude of hemispheric contrast in $\mathrm{SWABS}_{\mathrm{clr}}$, and the tropical precipitation is squeezed toward the equator. Indeed, a significant, albeit weak, correlation is found between the global-mean $\mathrm{SWABS}_{\mathrm{clr}}$ and SYM1-PC (Fig. S4b). Using the radiative kernels, we find that the spread of annual- and global-mean $\mathrm{SWABS}_{\mathrm{clr}}$ is not attributable to model differences in water vapor distribution, suggesting model differences in radiative transfer parameterizations as a likely cause (Fig. 5).

Among the components of NEI_0, the net surface energy flux in the equatorial region (SFC_0) is most strongly linked to SYM1-PC. The regression map of SFC onto SYM1-PC implies that a larger SYM1-PC is associated with a weaker atmospheric cooling over the equatorial upwelling region in the Pacific and Atlantic. A comparative analysis between CMIP and AMIP experiments suggests the importance of the ocean–atmosphere coupling particularly in the Pacific. We note that a causal relationship between SYM1-PC and SFC is not possible to discern from the correlation alone. For example, models with a smaller SYM1-PC would exhibit stronger trade winds, leading to a stronger equatorial upwelling. Regardless of the direction of causality, our results address the importance of improving model representation of cold tongue for correcting the simulated tropical precipitation pattern, consistent with previous studies (Li and Xie 2014; Adam et al. 2017).

To provide input on where focus could be most effectively applied in model development, we compare SYM1-PC of AMIP and CMIP. Weak but statistically significant correlation of 0.44 between the two (Fig. S6a) indicates that the variations among atmospheric components contribute to the precipitation bias in coupled models. As one of the candidates for biases to improve in atmospheric components, we consider model differences in annual- and global-mean SWABS whose similarity in magnitude and regression patterns between AMIP and CMIP experiments are stark (Fig. S6b and S7). The biases originating from the atmospheric component are exacerbated when coupled to a dynamic ocean—shown by larger inter-model spread of SYM1-PC in CMIP than AMIP experiments (Fig. S6a). Ocean–atmosphere interaction affects the net surface energy flux pattern in the deep tropics via modulation of the cooling strength over the equatorial upwelling regions (Fig. 6b), contributing to the symmetrical precipitation biases, consistent with Adam et al. (2017). Dissimilarity of the surface flux regression patterns between CMIP and AMIP (Fig. 6b, c) indicates that the bias in the Pacific is probably influenced by model differences in ocean dynamics or coupling processes.

This study focuses on the tropical precipitation pattern in the present-day climate state, but the analysis approach could be applied to understanding the factors controlling the future projections of tropical precipitation pattern. For example, the energetic constraints used to explain the symmetric pattern of present-day tropical precipitation spread can be similarly applied to explain the tropical precipitation squeeze pattern in global warming simulations (Lau and Kim 2015; Donohoe et al. 2019; Zhou et al. 2019). Furthermore, it is yet to be seen how the model bias in tropical precipitation affects the projected changes in tropical precipitation pattern.

Acknowledgements SMK and HK were supported by Basic Science Research Program through the National Research Foundation of Korea (NRF) funded by the Ministry of Science, ICT & Future Planning (2016R1A1A3A04005520). AGP was supported by the Regional and Global Model Analysis (RGMA) component of the Earth and Environmental System Modeling Program of the U.S. Department of Energy's Office of Biological & Environmental Research (BER) via NSF IA 1844590; NCAR is sponsored by the National Science Foundation (NSF) under Cooperative Agreement No. 1947282. AD's work was supported by the National Science Foundation Paleo Perspective on Climate Change (P2C2) Grant number AGS-1702827. All CMIP data were acquired from Earth System Grid Federation (ESGF) node hosted by Lawrence Livermore National Laboratory (LLNL). The authors express special thanks to all of the modeling groups who make CMIP data available and two anonymous reviewers for helpful comments.

References

Adam O, Bischoff T, Schneider T (2016a) Seasonal and interannual variations of the energy flux equator and ITCZ. Part I: zonally averaged ITCZ position. J Clim 29:3219–3230. https://doi.org/10.1175/JCLI-D-12-00467.1

Adam O, Schneider T, Brient F, Bischoff T (2016b) Relation of the double-ITCZ bias to the atmospheric energy budget in climate models. Geophys Res Lett 43:7670–7677. https://doi.org/10.1002/2016GL069465

Adam O, Schneider T, Brient F (2017) Regional and seasonal variations of the double-ITCZ bias in CMIP5 models. Clim Dynam. https://doi.org/10.1007/s00382-017-3909-1

Adler RF et al (2003) The version-2 global precipitation climatology project (GPCP) monthly precipitation analysis (1979-present). J Hydrometeorol 4:1147–1167. https://

doi.org/10.1175/1525-7541(2003)004%3c1147:TVGPCP%3e2.0.CO;2
Bellucci A, Gualdi S, Navarra A (2010) The double-ITCZ syndrome in coupled general circulation models: the role of large-scale vertical circulation regimes. J Clim 23:1127–1145. https://doi.org/10.1175/2009JCLI3002.1
Boccaletti G, Pacanowski RC, Philander SGH, Fedorov AV (2004) The thermal structure of the upper ocean. J Phys Oceanogr 34:888–902. https://doi.org/10.1175/1520-0485(2004)034%3c0888:Ttsotu%3e2.0.Co;2
Broccoli AJ, Dahl KA, Stouffer RJ (2006) Response of the ITCZ to Northern Hemisphere cooling. Geophys Res Lett. https://doi.org/10.1029/2005GL024546
Collins WD, Lee-Taylor JM, Edwards DP, Francis GL (2006) Effects of increased near-infrared absorption by water vapor on the climate system. J Geophys Res-Atmos. https://doi.org/10.1029/2005JD006796
De Szoeke SP, Xie SP (2008) The tropical eastern Pacific seasonal cycle: assessment of errors and mechanisms in IPCC AR4 coupled ocean—Atmosphere general circulation models. J Clim 21:2573–2590. https://doi.org/10.1175/2007JCLI1975.1
Dee DP et al (2011) The ERA-Interim reanalysis: configuration and performance of the data assimilation system. Q J R Meteor Soc 137:553–597
Donohoe A, Battisti DS (2013) The seasonal cycle of atmospheric heating and temperature. J Clim 26:4962–4980. https://doi.org/10.1175/Jcli-D-12-00713.1
Donohoe A, Marshall J, Ferreira D, Mcgee D (2013) The relationship between ITCZ location and cross-equatorial atmospheric heat transport: from the seasonal cycle to the last glacial maximum. J Clim 26:3597–3618. https://doi.org/10.1175/JCLI-D-12-00467.1
Donohoe A, Atwood AR, Byrne MP (2019) Controls on the width of tropical precipitation and its contraction under global warming. Geophys Res Lett 46:9958–9967. https://doi.org/10.1029/2019GL082969
Eyring V, Bony S, Meehl GA, Senior CA, Stevens B, Stouffer RJ, Taylor KE (2016) Overview of the coupled model intercomparison project phase 6 (CMIP6) experimental design and organization. Geosci Model Dev 9:1937–1958. https://doi.org/10.5194/gmd-9-1937-2016
Ham YG, Kug JS (2014) Effects of Pacific Intertropical Convergence Zone precipitation bias on ENSO phase transition. Environ Res Lett. https://doi.org/10.1088/1748-9326/9/6/064008
Hawcroft M, Haywood JM, Collins M, Jones A, Jones AC, Stephens G (2017) Southern Ocean albedo, inter-hemispheric energy transports and the double ITCZ: global impacts of biases in a coupled model. Clim Dynam 48:2279–2295. https://doi.org/10.1007/s00382-016-3205-5
Hirota N, Takayabu YN, Watanabe M, Kimoto M (2011) Precipitation reproducibility over tropical oceans and its relationship to the double ITCZ problem in CMIP3 and MIROC5 climate models. J Clim 24:4859–4873. https://doi.org/10.1007/s00382-013-1839-0
Hwang YT, Frierson DMW (2013) Link between the double-intertropical convergence zone problem and cloud biases over the Southern Ocean. Proc Natl Acad Sci USA 110:4935–4940. https://doi.org/10.1073/pnas.1213302110
Kang SM (2020) Extratropical influence on the tropical rainfall distribution. Curr Clim Change Rep 6:24–36
Kang SM, Held IM, Frierson DMW, Zhao M (2008) The response of the ITCZ to extratropical thermal forcing: idealized slab-ocean experiments with a GCM. J Clim 21:3521–3532. https://doi.org/10.1175/2007JCLI2146.1
Kang SM, Frierson DMW, Held IM (2009) The tropical response to extratropical thermal forcing in an idealized GCM: the importance of radiative feedbacks and convective parameterization. J Atmos Sci 66:2812–2827. https://doi.org/10.1175/2009JAS2924.1
Kang SM et al (2019) ETIN-mip extratropical-tropical interaction model intercomparison project-protocol and initial results. Bull Am Meteorol Soc 100:2589–2606. https://doi.org/10.1175/BAMS-D-18-0301.1
Kay JE, Wall C, Yettella V, Medeiros B, Hannay C, Caldwell P, Bitz C (2016) Global climate impacts of fixing the southern ocean shortwave radiation bias in the community earth system model (CESM). J Clim 29:4617–4636. https://doi.org/10.1175/JCLI-D-15-0358.1
Lau WKM, Kim KM (2015) Robust Hadley circulation changes and increasing global dryness due to CO_2 warming from CMIP5 model projections. Proc Natl Acad Sci USA 112:3630–3635. https://doi.org/10.1073/pnas.1418682112
Li G, Xie SP (2014) Tropical biases in CMIP5 multimodel ensemble: the excessive equatorial Pacific cold tongue and double ITCZ problems. J Clim 27:1765–1780. https://doi.org/10.1175/JCLI-D-13-00337.1
Li G, Du Y, Xu HM, Ren BH (2015) An intermodel approach to identify the source of excessive equatorial Pacific cold tongue in CMIP5 models and uncertainty in observational datasets. J Clim 28:7630–7640. https://doi.org/10.1029/2012GL053757
Lin JL (2007) The double-ITCZ problem in IPCC AR4 coupled GCMs: ocean–atmosphere feedback analysis. J Clim 20:4497–4525. https://doi.org/10.1175/Jcli4272.1
Mechoso CR et al (1995) The seasonal cycle over the tropical pacific in coupled ocean–atmosphere general-circulation models. Mon Weather Rev 123:2825–2838. https://doi.org/10.1175/1520-0493(1995)123%3c2825:Tscott%3e2.0.Co;2
Meehl GA, Covey C, Taylor KE, Delworth T, Stouffer RJ, Latif M, McAvaney B, Mitchell JFB (2007) The WCRP CMIP3 multimodel dataset: a new era in climate change research. Bull Am Meteorol Soc 88:1383–1394. https://doi.org/10.1175/BAMS-88-9-1383
Neelin JD, Held IM (1987) Modeling tropical convergence based on the moist static energy budget. Mon Weather Rev 115:3–12. https://doi.org/10.1175/1520-0493(1987)115%3c0003:Mtcbot%3e2.0.Co;2
Oueslati B, Bellon G (2015) The double ITCZ bias in CMIP5 models: interaction between SST, large-scale circulation and precipitation. Clim Dynam 44:585–607. https://doi.org/10.1007/s00382-015-2468-6
Pendergrass AG, Hartmann DL (2014) The atmospheric energy constraint on global-mean precipitation change. J Clim 27:757–768. https://doi.org/10.1175/Jcli-D-13-00163.1
Pendergrass AG, Conley A, Vitt FM (2018) Surface and top-of-atmosphere radiative feedback kernels for CESM-CAM5. Earth Syst Sci Data 10:317–324. https://doi.org/10.1175/Jcli-D-13-00163.1
Pincus R et al (2015) Radiative flux and forcing parameterization error in aerosol-free clear skies. Geophys Res Lett 42:5485–5492. https://doi.org/10.1002/2015gl064291
Schneider T, Bischoff T, Haug GH (2014) Migrations and dynamics of the intertropical convergence zone. Nature 513:45–53. https://doi.org/10.5065/D6F47MT6
Song XL, Zhang GJ (2018) The roles of convection parameterization in the formation of double ITCZ syndrome in the NCAR CESM: I. atmospheric processes. J Adv Model Earth Sy 10:842–866. https://doi.org/10.1002/2017ms001191
Takahashi K (2009) The global hydrological cycle and atmospheric shortwave absorption in climate models under CO_2 forcing. J Clim 22:5667–5675. https://doi.org/10.1175/2009jcli2674.1
Taylor KE, Stouffer RJ, Meehl GA (2012) An overview of Cmip5 and the experiment design. Bull Am Meteorol Soc 93:485–498. https://doi.org/10.1175/Bams-D-11-00094.1

Tian BJ (2015) Spread of model climate sensitivity linked to double-intertropical convergence zone bias. Geophys Res Lett 42:4133–4141. https://doi.org/10.1002/2015gl064119

Trenberth KE (1997) Using atmospheric budgets as a constraint on surface fluxes. J Clim 10:2796–2809. https://doi.org/10.1175/1520-0442(1997)010%3c2796:UABAAC%3e2.0.CO;2

Xiang B, Zhao M, Held IM, Golaz JC (2017) Predicting the severity of spurious "double ITCZ" problem in CMIP5 coupled models from AMIP simulations. Geophys Res Lett 44(3):1520–1527. https://doi.org/10.1002/2016GL071992

Xie PP, Arkin PA (1997) Global precipitation: a 17-year monthly analysis based on gauge observations, satellite estimates, and numerical model outputs. Bull Am Meteorol Soc 78:2539–2558. https://doi.org/10.1175/1520-0477(1997)078%3c2539:Gpayma%3e2.0.Co;2

Zhang XX, Liu HL, Zhang MH (2015) Double ITCZ in coupled ocean-atmosphere models: from CMIP3 to CMIP5. Geophys Res Lett 42:8651–8659. https://doi.org/10.1002/2015gl065973

Zheng YX, Shinoda T, Lin JL, Kiladis GN (2011) Sea surface temperature biases under the stratus cloud deck in the Southeast Pacific Ocean in 19 IPCC AR4 coupled general circulation models. J Clim 24:4139–4164. https://doi.org/10.1175/2011jcli4172.1

Zhou ZQ, Xie SP (2015) Effects of climatological model biases on the projection of tropical climate change. J Climate 28:9909–9917. https://doi.org/10.1175/Jcli-D-15-0243.1

Zhou W, Xie SP (2017) Intermodel spread of the double-ITCZ bias in coupled GCMs tied to land surface temperature in AMIP GCMs. Geophys Res Lett 44(15):7975–7984. https://doi.org/10.1002/2017GL074377

Zhou W, Xie SP, Yang D (2019) Enhanced equatorial warming causes deep-tropical contraction and subtropical monsoon shift. Nat Clim Change. https://doi.org/10.1038/s41558-019-0603-9